INTERNATIONAL JOURNAL FOR NUMERICAL METHODS IN FLUIDS
*Int. J. Numer. Meth. Fluids* 2002; **38**:985–1007 (DOI: 10.1002/fld.251)

# A high resolution upwind scheme for multi-component flows

D. Igra*,† and K. Takayama

*Shock Wave Research Center, Institute of Fluid Science, Tohoku University, Japan 2-1-1 Katahira, Aoba, Sendai 980-8577, Japan*

SUMMARY

Conservative schemes usually produce non-physical oscillations in multi-component flow solutions. Many methods were proposed to avoid these oscillations. Some of these correction schemes could fix these oscillations in the pressure profile at discontinuities, but the density profile still remained diffused between the two components. In the case of gas–liquid interfaces, density diffusion is not acceptable. In this paper, the interfacial correction scheme proposed by Cocchi *et al.* was modified to be used in conjunction with the level-set approach. After each time step two grid points that bound the interface are recalculated by using an exact Riemann solver so that pressure oscillations and the density diffusion at discontinuities were eliminated. The scheme presented here can be applied to any type of conservation law solver. Some examples solved by this scheme and their results are compared with the exact solution when available. Good agreement is obtained between the present results and the exact solutions. Copyright © 2002 John Wiley & Sons, Ltd.

KEY WORDS: gas–liquid interface; level-set approach; compressible flow; numerical scheme

## 1. INTRODUCTION

Shock capturing schemes such as TVD or ENO are usually useful to accurately simulate single component gas flows. However, in the case of multi-component flow, consisting of two foreign gas interfaces or two-phase flows, non-physical pressure fluctuations usually appear in the solution across gaseous interfaces. These pressure fluctuations are created as a result of the calculation of pressures from an equation of state based on the total energy in the gas. In multi-component flows, even when the densities and velocities are initially identical, the internal energy of each fluid will be different due to the difference in their specific heat ratios $\gamma$, and hence at one time step the energy diffusion across the interface will appear. This discontinuity in $\gamma$ across the interface will cause an incorrect value for the pressure to be calculated at the interface. In the next time step, a false velocity will subsequently be calculated since its derivation was based on the incorrect pressure value.

*Correspondence to: D. Igra, Shock Wave Research Center, Institute of Fluid Science, Tohoku University, Katahira 2-1-1, Aoba, Sendai 980-8577, Japan.
†E-mail: dan@ceres.ifs.tohoku.ac.jp

*Received December 1999*
*Revised 16 October 2000*

To date many researchers, Abgrall [1], Cocchi and Saurel [2], Cocchi *et al.* [3], Jenny *et al.* [4], Karni [5, 6], Shyue [7] have proposed possible methods to overcome this problem. Karni [6] proposed to solve the pressure evolution equation across the material interface. By using this type of pressure calculation a smooth pressure profile was obtained across the interface without calculating the pressure based on the equation of state. Others suggested use of a variety of quasi conservative schemes, e.g. Abgrall [1] Shyue [7]. In their schemes, the density change across the interface was diffusive. In most schemes the shock discontinuities are typically smeared over 2–3 grid points while the interface is smeared over 5–7 grid points. When dealing with gas phase only, the smearing could be acceptable. However, when dealing with two phase flows such as gas and liquid phases with an accompanying large density change between these two phases, any density diffusion across the interface is strictly unacceptable. No mixing takes place between gas–liquid interfaces except in very special cases. Thus, numerical diffusions could result in unphysical densities at the interfaces. Therefore, a different method should be employed to overcome this unphysical mixing by eliminating pressure fluctuations at the interface and keeping a discontinuous density profile at the interface. Cocchi *et al.* [3], Cocchi and Saurel [2] managed to achieve these goals by employing a Godunov scheme coupled with a front tracking method. Their scheme uses results derived from the exact Riemann solver for correcting the density diffusion and pressure fluctuations at the interface. The pressure and density are corrected at the grid points across the interface. Therefore, the numerical density diffusion and pressure oscillations are removed.

The work presented in this paper improves the existing scheme by changing the interface tracking from a front tracking method to a front capturing scheme using the level-set approach. Mulder *et al.* [8] employed the level-set approach for gas dynamic problems. They studied two gas interface instabilities, so it was not required to preserve a sharp density gradient at the interface. Therefore a Roe approximate Riemann solver for ideal gas equation of state was employed. They used the level-set approach to track the interface position and follow its evolution. Their method can be readily added to any schemes which are based on the approximate Riemann solver such as TVD and ENO schemes for solving gas flows based on the ideal gas equation of state. It can handle the separation or merger of interfaces, which are difficult to perform with a front tracking method. In addition, the front tracking method is more computationally demanding than the level-set approach which requires only one additional equation to be added to the computational model.

The basic outline of the present scheme is to use a TVD scheme with the level-set approach for solving the flow field under study. After each iteration, application of the correction step to the grid points on both sides of the interface is employed. This is performed using an exact Riemann solver similar to Cocchi *et al.* [3]. For one-dimensional problems this method is similar to that used by Cocchi *et al.* [3]. However, in the present procedure the correction step has been improved for some cases and is modified to be used with the level-set approach. This method is simpler in its application to the two-dimensional problems than the front tracking method and provides better results for the separation and merger of interfaces.

The outline of this paper is as follows: In Section 2 a description of the numerical scheme is given. It contains a brief description about the level-set approach. A TVD scheme for two fluids incorporating the level-set approach for tracking the interface is developed. Then the corrector step employed to correct the pressure oscillation and density diffusion across the material interfaces is presented; numerical examples are given in Section 3; Finally conclusions are presented in Section 4.

 

## 2. THE NUMERICAL SCHEME

### 2.1. Level-set approach

Mulder *et al.* [8] present a TVD scheme incorporating the level-set approach to track the interface between two gases. The level-set approach is an interface capturing scheme based on level-set functions. It can capture the interface between two grid points. Let the level-set function $\psi$ be defined as the distance between a grid point and the interface. $\psi = 0$ designates the material interface. Then positive $\psi$ designates one material and negative $\psi$ designates the other material. Knowing the value of $\psi$ the specific heats ratio can be defined as a function of the level-set function.

$$\gamma(\psi) = \begin{cases} \gamma, \psi > 0 & \text{gas} \\ n, \psi < 0 & \text{liquid} \end{cases} \tag{1}$$

The level-set function propagates with the local fluid velocity and can be written as the advection equation in the non-conservative or conservative form.

$$\psi_t + u\psi_x = 0 \tag{2}$$

or

$$(\rho\psi)_t + (u\rho\psi)_x = 0 \tag{3}$$

Equations (2) and (3) have their advantages and drawbacks. Some examples of these will be presented in Section 3 and are also demonstrated by Mulder *et al.* [8]. The non-conservative form (2) will produce better results in the cases where two fluids with large density ratio advect at a constant velocity. However, for large velocity fluctuations which occur in a shock tube flow, it might produce a wrong interface position (for details see Section 3). Its main advantage is that the density is not coupled with the level-set functions as in Equation (3). Using the conservative formulation might create large gradients in the level-set functions in the case of two fluids having a large density ratio, such as a gas–liquid interface. When calculating flows with large density gradients some numerical diffusion could appear at the material interface that can lead to an incorrect position of the material interface in an advection calculation at a constant velocity. However, when (3) is used for the calculation of a shock tube problem the conservative level-set approach can give the correct position of the material interface. In addition, (3) has the advantage that it can readily be added to any system of hyperbolic conservation solvers. For these two reasons the decision was made to employ it in the present computations.

The location of the interface can readily be by found satisfying the following equation:

$$\psi_i \psi_{i+1} < 0 \tag{4}$$

where the interface is located between grid points $i, i+1$. Next the level-set propagation equation will be incorporated into a system of hyperbolic conservation laws.

### 2.2. Incorporating the level-set approach with the approximate Riemann solver

An equation of state for each component is required, it is an important part of any exact or approximate Riemann solver. This is not necessarily a straight forward step since a different

 

equation of state is needed for each fluid. When simulating gas–liquid interface, finding a suitable equation of state for both phases is quite problematic. One equation of state that is widely employed is the stiffened gas equation of state since it can be used to describe both the gas and the liquid. It has been used by Cocchi *et al.* [3], Cocchi and Saurel [2] and Shyue [7] for calculating gas–liquid interfaces. Further information about this type of equation of state can be found in Menikoff and Plohr [9]. The total energy per unit of volume is

$$E = \frac{p + \gamma B}{(\gamma - 1)} + \frac{1}{2}\rho u^2 \tag{5}$$

where $p$ is the pressure, $\rho$ is the density, $B$ and $\gamma$ are parameters for water, $\gamma = 7.415$ and $B = 296.3\,\text{MPa}$. When this equation is used for gases, $B$ is set to zero and $\gamma$ is equivalent to the specific heat ratio, where for air, $\gamma = 1.4$. It is possible to employ any equation of state as long as both the Riemann solvers are updated accordingly. Here an approximate Riemann solver was modified to incorporate the stiffened gas equation of state and the level-set approach. The proposed solver is based on that by Mulder *et al.* [8].

The Euler equations including the level-set function, are written in vector form as follows:

$$\begin{pmatrix} \rho \\ \rho u \\ E \\ \rho\psi \end{pmatrix}_t + \begin{pmatrix} \rho u \\ \rho u^2 + P \\ u(E + P) \\ \rho u\psi \end{pmatrix}_x = 0 \tag{6}$$

where $\rho$ is the density, $u$ is the velocity, $p$ is the pressure, $E$ is the total energy per unit of volume and $\psi$ is the level-set function.

The Jacobian matrix in this case is

$$A = \begin{pmatrix} 0 & 1 & 0 & 0 \\ \dfrac{\gamma - 3}{2}u^2 - \psi\chi & (3 - \gamma)u & (\gamma - 1) & \chi \\ \dfrac{\gamma - 3}{2}u^3 - uH - u\psi\chi & H - (\gamma - 1)u^2 & \gamma u & u\chi \\ -u\psi & \psi & 0 & u \end{pmatrix} \tag{7}$$

where $H$ is the enthalpy and $\chi = (\partial p/\partial\rho)|_\varepsilon$ which is the derivative of pressure as a function of density while the internal energy is kept constant.

The eigenvalues of the Jacobian matrix $A$ are:

$$\lambda_1 = u + c, \quad \lambda_2 = \lambda_3 = u, \quad \lambda_4 = u - c \tag{8}$$

where $c$ is the speed of sound, defined as

$$c = \sqrt{\frac{\gamma(p + B)}{\rho}} \tag{9}$$

 

The eigenvectors are:

$$r_1 = \begin{pmatrix} 1 \\ u+c \\ H+uc \\ \psi \end{pmatrix}, \quad r_2 = \begin{pmatrix} 1 \\ cu \\ \frac{1}{2}u^2 \\ \psi \end{pmatrix}, \quad r_3 = \begin{pmatrix} 0 \\ 0 \\ \dfrac{-\chi}{\gamma-1} \\ 1 \end{pmatrix}, \quad r_4 = \begin{pmatrix} 1 \\ u-c \\ H-uc \\ \psi \end{pmatrix} \tag{10}$$

A local flow fluctuation $\Delta W = W_R - W_L$ can be projected onto the characteristic field $\Delta W = \sum_i \alpha_i r_i$ where the local wave strengths are:

$$\alpha_1 = \frac{\delta p - \rho c \delta u}{2c^2}, \quad \alpha_2 = \frac{c^2 \delta\rho - \delta p}{c^2}, \quad \alpha_3 = \rho\delta\psi, \quad \alpha_4 = \frac{\delta p + \rho c \delta u}{2c^2} \tag{11}$$

Having this information one can proceed and use any type of solver for solving the flow field under consideration. In the present work the Harten [10] and Yee [11] modified flux TVD scheme is used. Other schemes may also be used. The first step is to write Roe's approximate Riemann solver for multi-component flows. We begin with the basic Roe's averages which are:

$$\rho^* = \sqrt{\rho_L \rho_R} \tag{12}$$

$$u^* = \frac{\sqrt{\rho_L}u_L + \sqrt{\rho_R}u_R}{\sqrt{\rho_L \rho_R}} \tag{13}$$

$$H^* = \frac{\sqrt{\rho_L}H_L + \sqrt{\rho_R}H_R}{\sqrt{\rho_L \rho_R}} \tag{14}$$

$$\psi^* = \frac{\sqrt{\rho_L}\psi_L + \sqrt{\rho_R}\psi_R}{\sqrt{\rho_L \rho_R}} \tag{15}$$

Similar to the approach of Mulder *et al.* [8] Equation (17), is defined as the variable that represents changes in energy due to changes of phase or fluid. The same equation has been previously employed by Mulder *et al.* [8], Karni [5]. Further details regarding this equation can be found in Mulder *et al.* [8]. It is based on $\gamma^*$ which must be approximated first Equation (18).

$$c^* = \sqrt{(\gamma^* - 1)(H^* - \tfrac{1}{2}u^{*^2})} \tag{16}$$

$$\chi^* = \frac{(p_R - p_L) - (\gamma^* - 1)(((p + \gamma B)/(\gamma - 1))|_R - ((p + \gamma B)/(\gamma - 1))|_L)}{\rho^*(\psi_R - \psi_L)} \tag{17}$$

$$\gamma^*(\psi^*) = \frac{(\psi^* - \psi_L)\gamma_R - (\psi_R - \psi^*)\gamma_L}{\psi_R - \psi_L} \tag{18}$$

Once the approximate Riemann solver has been defined, any scheme can be used to calculate the numerical flux.

 

The above scheme can be used for multi-component calculations. However, Karni [5] proved that such a scheme produces large errors of first order magnitude, at the material interface between two gases. The errors are generated due to the sharp change in $\gamma$ at the interface and result in pressure fluctuations. These cause fluctuations in all other flow variables. Therefore, a correction scheme is required to obtain the correct solution at the material interface; this will be described next.

### 2.3. Correction step

The interface correction step is based on that proposed by Cocchi *et al.* [3], Cocchi and Saurel [2]. The main idea in this approach is that the two grid points just in front and behind the interface are recalculated in the corrector step using an exact Riemann solver. The results obtained from the exact Riemann solver are used for updating the values in the two grid points across the interface; thus, a sharp density gradient is maintained. There are two types of correction steps depending upon the location of the interface at time step $n+1$. The first is used when the interface remains within the same two grid points. The other is used when the interface moves forward or backward, i.e. one of the two previous grid points is changed. For example at time step $n$, the interface was located between grid point $i, i+1$, while at time step $n+1$ the interface is located between grid points $i+1,\ i+2$. For each case a different interface correction step is utilized. An outline of the correction step is as follows; first, the location of the interface at time $n$ between grid points $i, i+1$ is found using (4). This procedure was described in Section 2.1; when $\psi_{i+1}^n \psi_i^n < 0$ the interface is located between the grid points $i$ and $i+1$. The second step is to calculate an exact Riemann solver for grid points $i, i+1$ using the stiffened gas equation of state.

The correction step, when the interface is still located between grid points $i, i+1$, is presented first. The interface location at the next time step $n+1$ can readily be found using Equation (4) with the level-set functions for time step $n+1$. Based on the level-set function the interface location ($\psi = 0$) was interpolated by using the following equation:

$$x_{mi} = \frac{|\psi_i^{n+1}|}{|\psi_{i+1}^{n+1}| + |\psi_i^{n+1}|} \Delta x + x_i \tag{19}$$

The interface location is needed to calculate the new values of the grid points on both sides of the interface. This value is interpolated from the results of the exact Riemann solver with results from the TVD solver at time step $n+1$ using the following equations:

$$U_i^{n+1} = \frac{x_i - x_{i-1}}{x_{mi} - x_{i-1}} (U_1^* - U_{i-1}^{n+1}) + U_{i-1}^{n+1} \tag{20}$$

$$U_{i+1}^{n+1} = \frac{x_{i+1} - x_{i+2}}{x_{mi} - x_{i+2}} (U_r^* - U_{i+2}^{n+1}) + U_{i+2}^{n+1} \tag{21}$$

where values marked with a star are obtained from the exact Riemann solver and include either left or right propagating waves. These Equations (20) and (21) are similar to those of Cocchi *et al.* [3] except that here the interface location is determined by using the level-set functions.

 

The other correction step is used when the interface propagates to a new location. For example, at time step $n+1$ it is located between grid points $i+1, i+2$ or $i, i-1$; by using Equation (4) with the level-set function calculated for time step $n+1$, the new location of the interface can be determined. The corrector step as given by Cocchi, Saurel *et al.* [3] for the case when the interface propagates forward is

$$U_{i+1}^{n+1} = U_1^* \tag{22}$$

In addition, the parameters $\gamma$ and $B$ of the equation of state are updated according to the position of the interface corresponding to the values of the level-set function at time step $n+1$. This is performed using Equation (1).

However, here the other grid point must be corrected as well, otherwise it will remain diffused. This correction is not included in the procedure employed by Cocchi *et al.* [3]. To demonstrate the importance of this correction step a gas–liquid interface propagating at a constant velocity will be discussed. At the time step $n+1$, the interface location has moved to a new location between grid points $i+1$ and $i+2$. The correction step is applied and the liquid parameters at grid point $i+1$ are obtained. However, the liquid at grid point $i$ is slightly diffused due to the previous interface location; it has lower density and energy than it had previously, at time step $n$. Therefore, one must correct the results at grid point $i$ as well as those at grid point $i+1$, otherwise numerical errors are created.

We define the following correction for grid point $i$:

$$U_i^{n+1} = \tfrac{1}{2}\,(U_1^* + U_{i-1}^{n+1}) \tag{23}$$

Now that the corrector step has been defined a few solutions to the one-dimensional flows based on the above scheme shall be presented.

## 3. NUMERICAL EXAMPLES

The present section contains a few numerical examples of one-dimensional flows. The solutions obtained are compared with results of other researchers [1–3] and with the exact solution when available. It is shown that employing the proposed scheme produces accurate results, especially near the interface.

### *3.1. Example 1: Two gas shock tube*

The first example is taken from Abgrall [1]. This is a classical shock tube flow where helium is the driver gas and air is the driven gas. In two-gas interface mixing is possible, however using the above scheme which was designed for immiscible fluids results in a sharp density discontinuity between the two gases. In this example, a uniform grid of 100 points was used. The CFL number is 0.9 and the initial conditions are given in Table I.

Abgrall [1] has shown that solving this example creates a density oscillation at the two-gas interface. Abgrall [1] even had a very small velocity kink at the interface. Therefore, it is worth testing this problem with the present scheme. The results shown in Figure 1 use a superbee limiter for the linear fields and a Van Leer limiter for the non-linear fields. The results for pressure and velocity are continuous across the interface. They agree well with the exact solution and the interface location is captured correctly.

 

Table I. Initial conditions for example 1.

| | Density ($Kg/m^3$) | Pressure (bar) |
|---|---|---|
| Helium (left) | 14.54903 | 194.3 |
| Air (right) | 1.16355 | 1 |

Next the superbee limiter was used for all fields, the results for this case are shown in Figure 2. When compared with Figure 1, the density profile shows slightly better agreement with the analytical solution near the interface and a sharp density gradient at the interface is observed. However, at $x = 0.5$ a slight density increase appears, which is probably caused by the compressibility effects of the superbee limiter Yee [11]. The numerical velocity and pressure obtained with this limiter agree well with the exact solution.

In the next example a one step non-conservative scheme is used to calculate the level-set functions, which has second-order accuracy both in time and in space. A minmod limiter is employed in this example as well. The result is shown in Figure 3. The main difference between this calculation and the previous one is that the interface location is shifted by about 2 grid points. Except for this discrepancy good agreement is obtained between the present results and the exact solution. The error in the interface location is created on account of the level-set function being calculated in a non-conservative form. In the problems under study there is a large velocity change at the interface at the initial stage when the 'diaphragm' between the high and low pressure sections ruptures. At first the velocity changes are large and might result in this type of error. A higher order solver might improve the result, since Mulder *et al.* [8] captured the interface location using a multi step non-conservative scheme.

### *3.2. Example 2: Hydrodynamic shock tube*

This example is a hydrodynamic shock tube taken from Cocchi *et al.* [3]. The initial conditions are given in Table II. The driver gas is pressurized air and the driven section is filled with water. A minmod limiter and $CFL = 0.9$ are used. The calculations were performed on uniform grid of 100 points. The interface location is captured accurately in spite of the diffusive limiter that was employed in this example.

The results obtained are shown in Figure 4. Good agreement between the numerical results and the exact solution near the gas–liquid interface is shown. As expected the pressure and velocity are continuous across the interface. Near the expansion wave their agreement is not good mainly due to the use of the diffusive minmod limiter. In other locations in the flow field the agreement between the numerical flow variables and the exact solution is very good.

Based on the one-dimensional examples presented so far, it is possible to estimate the error of the interface location by comparing the numerical results with the exact solution. This comparison is carried out for the results shown in Figures 1, 2 and 4. In these cases the level-set functions were calculated in a conservative form. The interface location was calculated using Equation (19). The error is defined as the difference between the interface location as derived from the exact solution and that calculated based on the level-set approach. The results of this calculation are shown in Table III. The error in all the calculations is smaller than $\Delta x$ which is 0.01 indicating that the interface location was captured with at least first-order accuracy.

 

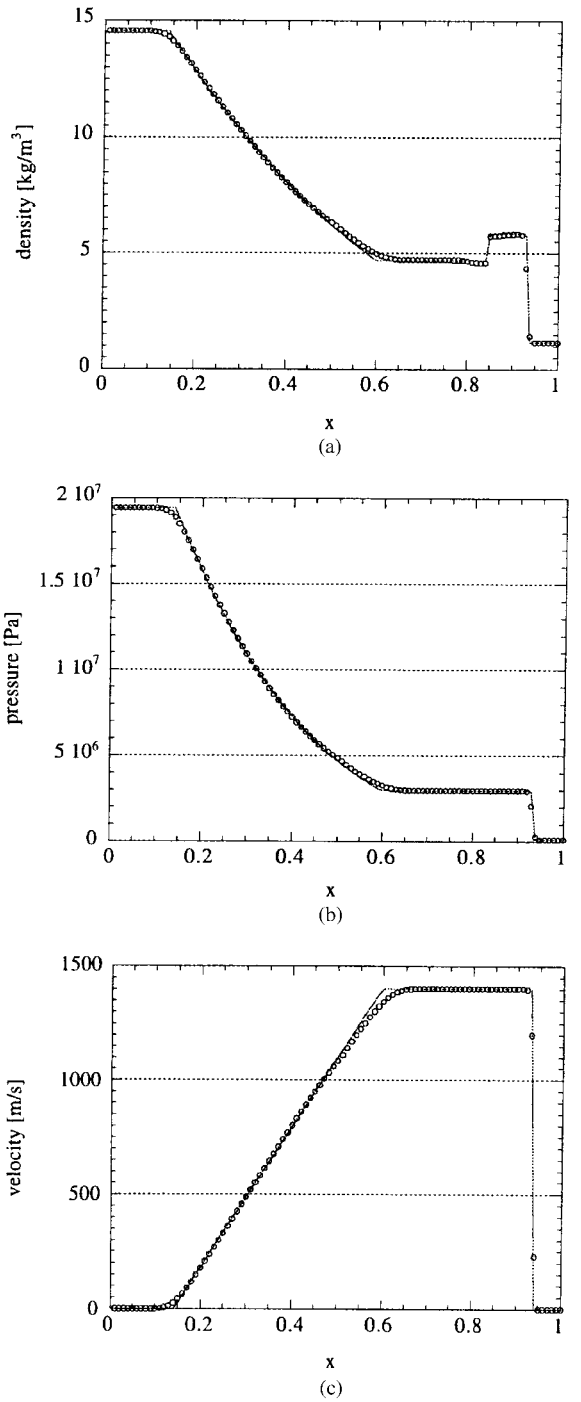


Figure 1. Example 1, $\psi$ is calculated in conservative formulation Superbee limiter for linear waves, CFL=0.9.

 

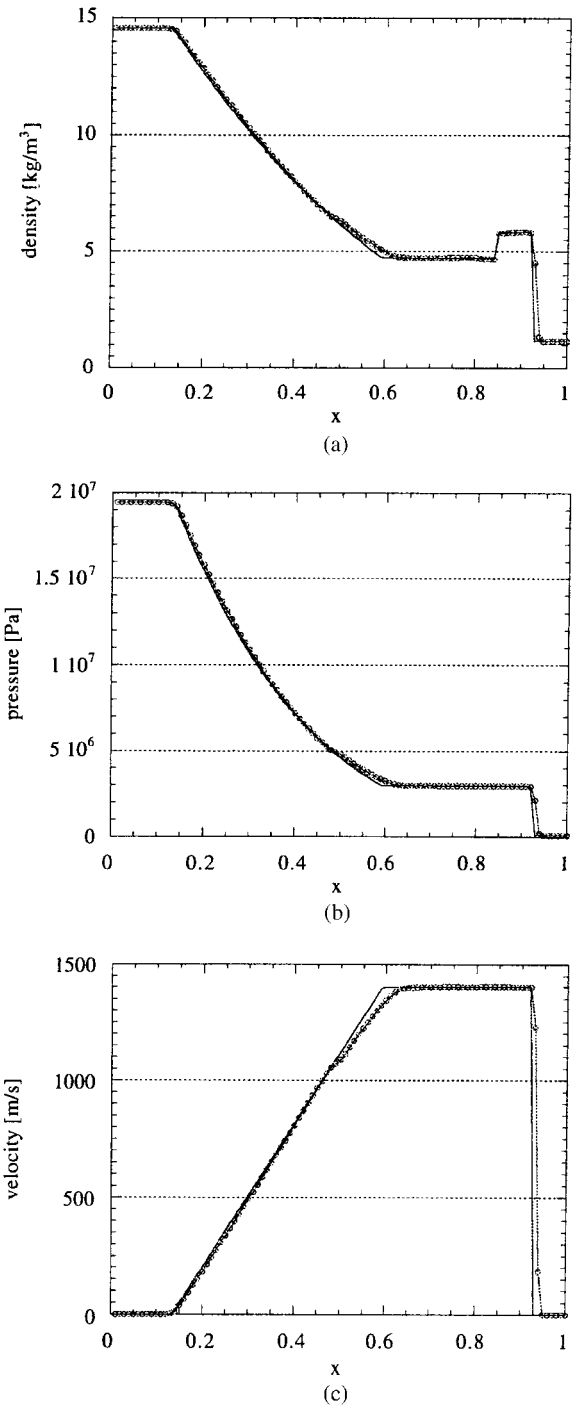


Figure 2. Example 1, $\psi$ is calculated in conservative formulation Superbee limiter, CFL = 0.9.

 

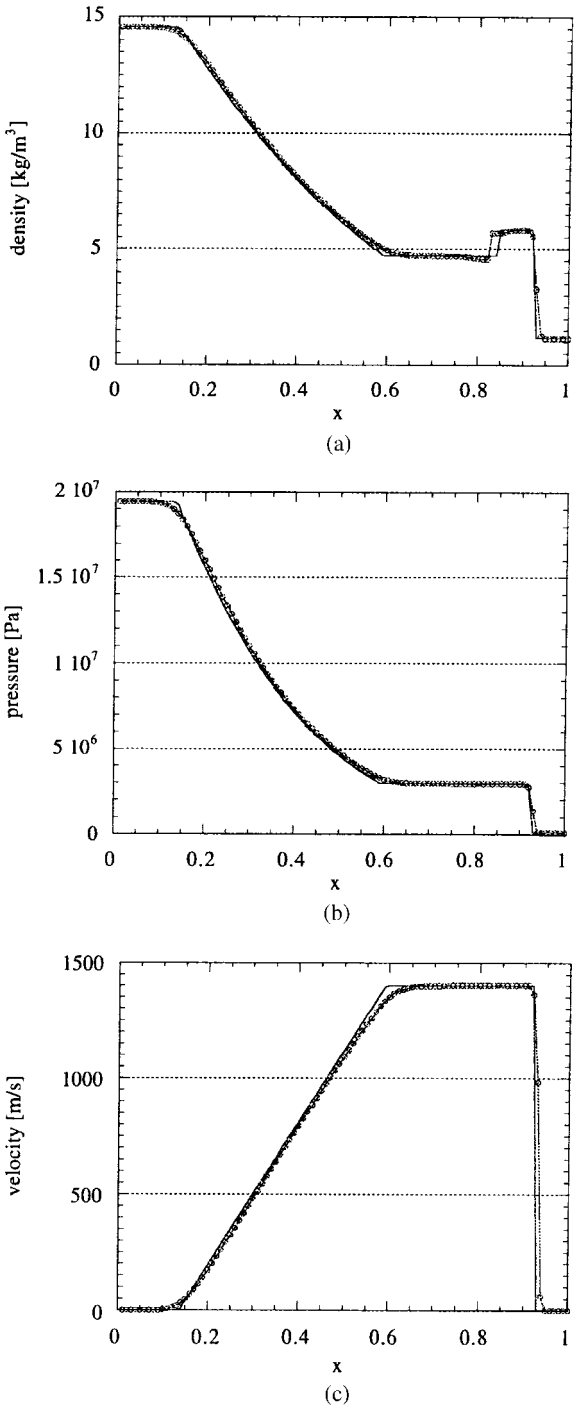


Figure 3. Example 1, $\psi$ is calculated in non-conservative formulation minmod limiter, CFL = 0.9.

 

Table II. Initial conditions for example 2.

| | Density ($Kg/m^3$) | Pressure (bar) |
|---|---|---|
| Air (left) | 1254 | 9000 |
| Water (right) | 1000 | 1 |

### 3.3. *Example 3: Interaction of two blast waves in water*

This test case is based on the example presented by Woodward and Colella [12]. They originally calculated the interaction of two strong blast waves in air. Initially the flow field is divided into three parts. The length of the left and right sections is 10% of the total flow field. They contain high pressure air while the central part contains low pressure air. The high pressure regions create blast waves in the central part which interact with each other. Ivings *et al.* [13] calculated a similar problem with three different gases filling each part of the initial flow field as [12].

Here the central part is filled with ambient water, two strong blast waves in air interact in water. At both ends of the flow field, solid boundaries are imposed therefore the waves are reflected back into the flow field. The initial conditions are as follows:

high pressure air of $10^{10}$ Pa and density of $1.25\,kg/m^3$ at $x < 0.1$ m
high pressure air of $10^9$ Pa and density of $1.25\,kg/m^3$ at $x > 0.9$ m

The parts of high pressure air sandwich the water part at $10^5$ Pa and the density of $1000\,kg/m^3$. Initially all the parts are quiescent. The calculation field is 1 m long and was divided into 2000 equally spaced grid points. The CFL number is 0.9 and a minmod limiter is used.

In Figure 5 isopycnics show the blast wave propagation in the $x$–$t$ diagram. The blast waves (B1–B4) and contact surfaces $(C, I)$ are clearly visible. At about 90 μs a complex wave interaction takes place. The two blast waves (B1, B2) collide with each other creating a new series of waves (B3, B4, C). At about 125 μs the right blast wave (B3) interacts with the gas–liquid interface generating another wave system (T).

When the diaphragms are instantaneously removed at both sides, two strong blast waves propagate into the water. At the same time, two rarefaction waves propagate in the opposite direction into the air. These waves are later reflected off the solid boundary and propagate back into the water. The wave on the left side (B1) interacts first since, due to its higher initial pressure, it propagates faster. The interaction can be seen in Figure 6, where a density jump at the shock wave is present at $x = 0.2$ m. A similar wave appears at the right-hand side (B2); however, it is weaker due to its lower initial pressure. Previously Woodward and Colella [12], Ivings *et al.* [13] studied only gaseous phase flow. In those simulations when a rarefaction wave interacted with a contact discontinuity, it was reflected from the contact surface and only a minute amount of energy was transmitted to the lower pressure gas. In the present case, on the contrary, the acoustic impedance of the high pressure gas and that of the low pressure water are in a similar order of magnitude. Therefore, each time when a rarefaction wave is reflected from the contact discontinuity, a larger partial energy is transmitted into

 

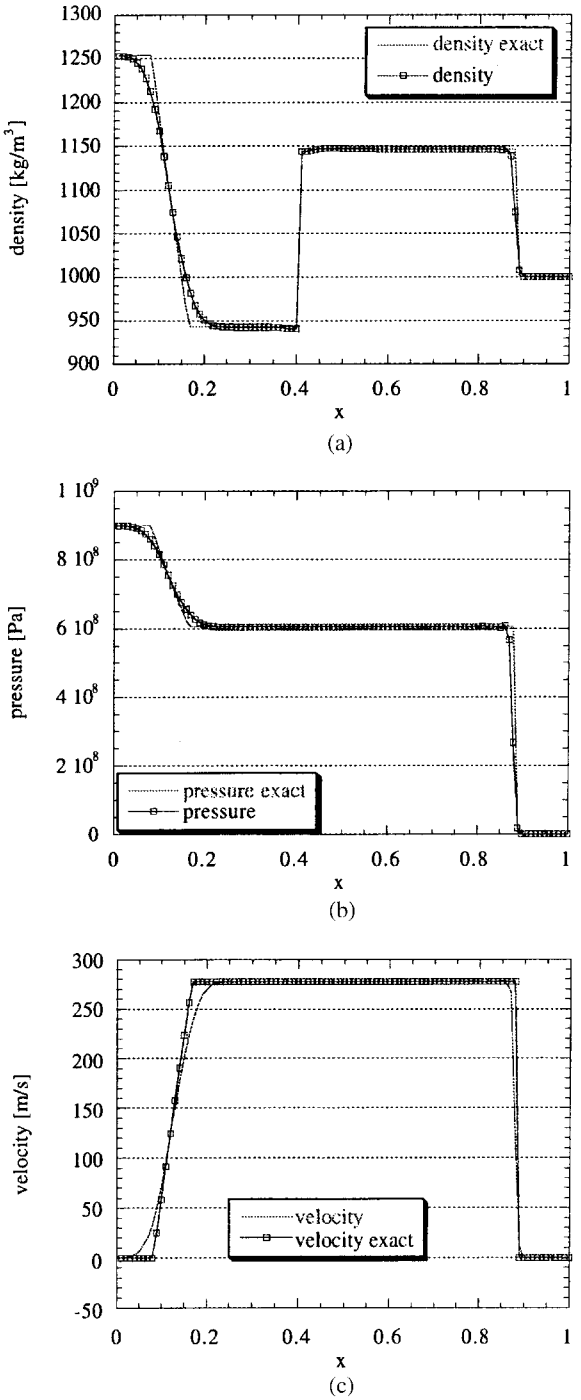


Figure 4. Example 2, air water Riemann problem, minmod limiter CFL = 0.9.

 

Table III. Interface location error analysis.

| Type | Exact location | Location of $\psi_{mi} = 0$ | Error (exact $- \psi_{mi}$) |
|---|---|---|---|
| He-air combination limiter | 0.84696 | 0.8408635 | $-6 \times 10^{-3}$ |
| He-air superbee limiter | 0.8483462 | 0.84123 | $7.116 \times 10^{-3}$ |
| Air water minmod limiter | 0.4002784 | 0.3972799 | $2.9985 \times 10^{-3}$ |

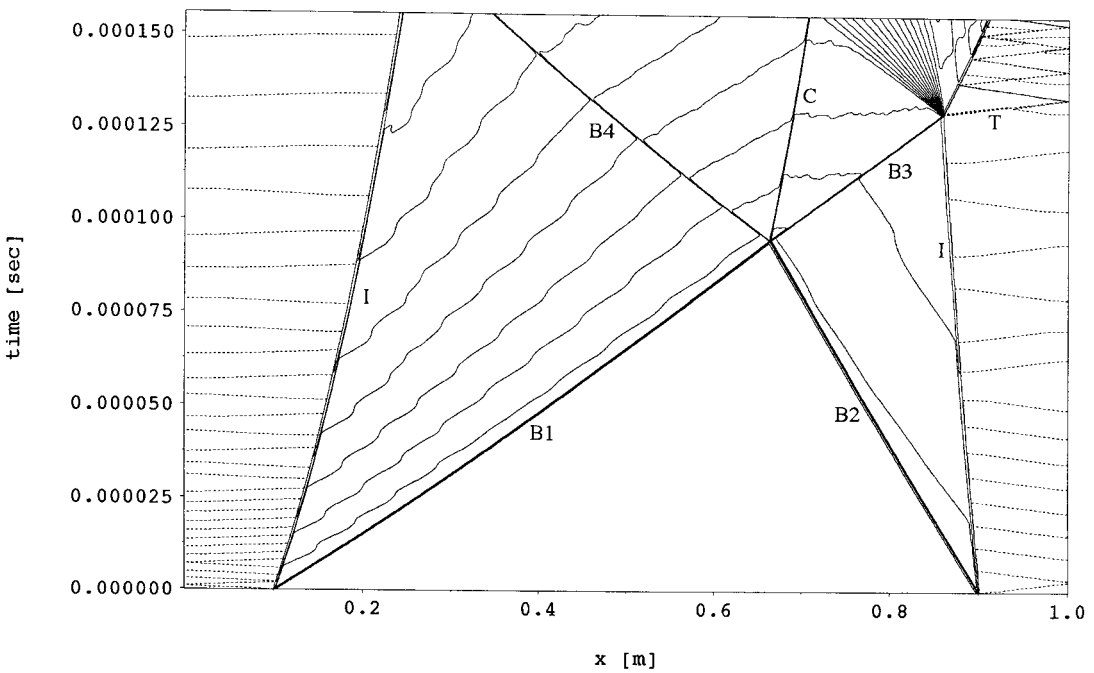


Figure 5. Density contours in space and time. The solid lines are water of density 1000–1575 with equal steps every 25 (kg/m$^3$). The dashed lines are air with density values of 0.5–1.52 with equal steps every 0.025 (kg/m$^3$).

the water. Those transmitted waves create the 'staircase-like' set of waves appearing at all stages of the present simulation. These are especially noticeable in the velocity and pressure fields.

Another difference observed between the present case and the previous ones where only gases were involved is the maximum density experienced in the water after its initial interaction with the blast waves. In air, the maximum achievable density on both sides is similar due to the limitation of the maximum density ratio in gases. For air this ratio is at most 6 times larger than the initial density. In water however, the density on the left side is higher than that on the right side. To achieve similar densities on both sides of water a much higher

 

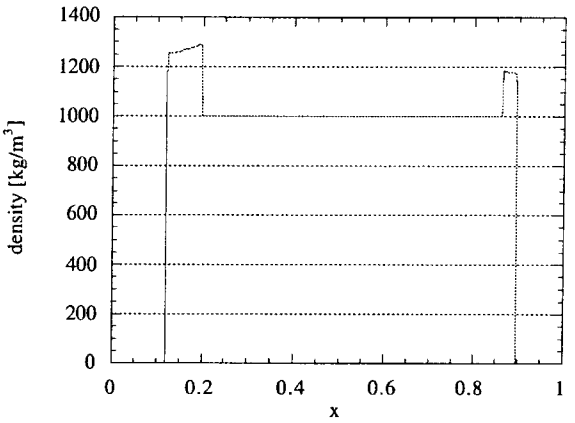


(a)

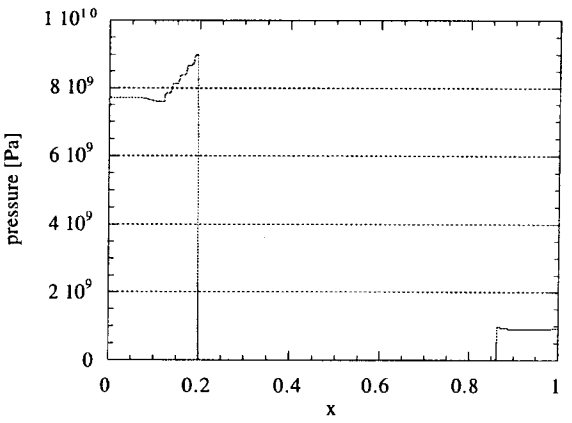


(b)

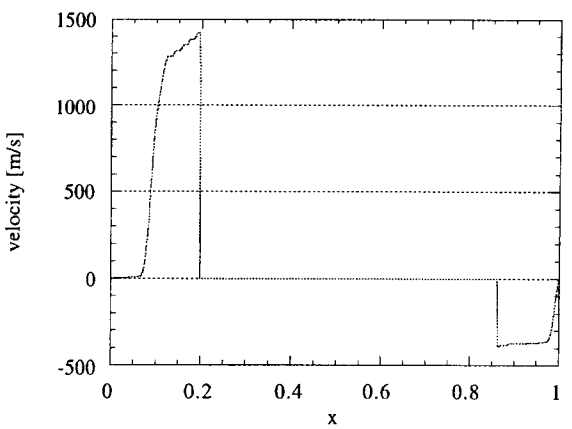


(c)

Figure 6. Flow field at $t = 15$ (μs).

 

initial pressure is required. Therefore, the water densities behind each blast wave are different in the present simulation.

At the next time step shown in Figure 7, the two blast waves propagate towards each other. With the elapse of time the rarefaction wave on the left-hand side interacts more strongly with the contact surface than that on the right, resulting in stronger transmitted waves that are more easily observed. There are more waves appearing on the left-hand side due to the higher pressure jump across the left-hand side blast wave. Therefore, it has a higher sound speed and the waves propagation speed is higher there. In addition, this higher initial pressure causes the interface on the left-hand side to bend more than that on the right-hand side, as seen in Figure 5.

Figure 8 shows the flow field just before the blast waves (B1, B2) collide with each other at about $x = 0.66$ m. This can be determined from the fact that the water density is still close to its initial value at about $x = 0.67$ m. Very large changes in pressure and density are also found near this location. A short time later, the collision between the two blast waves results in pressure and density peaks as seen in Figure 9, which disappear at a later time due to a dissipation process.

In Figure 10 the stronger blast wave (B3) continues to propagate to the right, at this time it is located at about $x = 0.71$ m. At the same time the weaker wave (B4) propagates to the left which can be seen at about $x = 0.61$ m. In between these waves, a contact discontinuity (C) is generated. As these waves propagate in opposite directions, their pressure and density values decrease.

At a later time, the stronger blast wave (B3) interacts with the right interface as seen in Figure 11. As a result a weak shock wave (T) is transmitted into the air while an expansion wave is created in the water. This behaviour is similar to the case in which an underwater shock wave interacts with a gas bubble, see Cocchi and Saurel [2] for more details. Figure 11 shows the contact discontinuity (C) and the weak blast wave (B4) continuing to propagate to the left. The transmitted wave in air has a very high velocity. This is due to the high pressure generated in air by the blast wave that results in a high speed of sound. A velocity peak can be seen in Figure 11 at about $x = 0.92$ m. Once this wave reaches the wall it is reflected back to the gas–liquid interface where some fraction of its energy is transmitted to the water, creating a new 'staircase like' wave structure as seen in Figure 12. This wave then reflects off the gas–liquid interface and propagates back towards the wall. This process continues until the end of the present simulation. At ($t = 151.5$ μs shown in Figure 12), the rarefaction wave in the water can be clearly seen. This wave was generated when the blast wave (B1) first interacted with the left gas–liquid interface.

## 4. CONCLUSIONS

As is clearly evident from the numerical examples, the proposed scheme is suitable for handling gas–liquid interfaces. It does not create pressure oscillation or density diffusion at the interface. The interface was captured using the level-set approach which was added to the system of conservation laws. This system can be solved by employing any type of solver. A correction scheme based on Cocchi and Saurel [2], Cocchi *et al.* [3] was used. It was modified to be employed with the level-set approach and a moving interface.

 

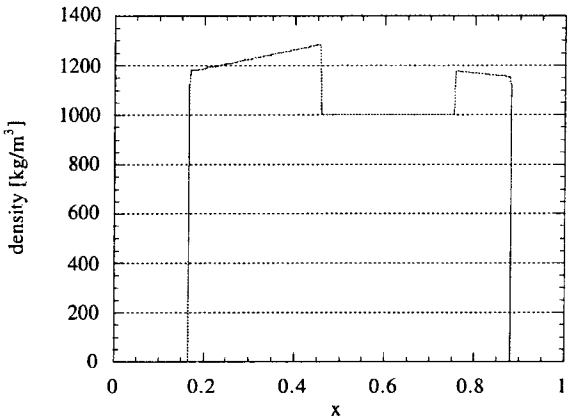


(a)

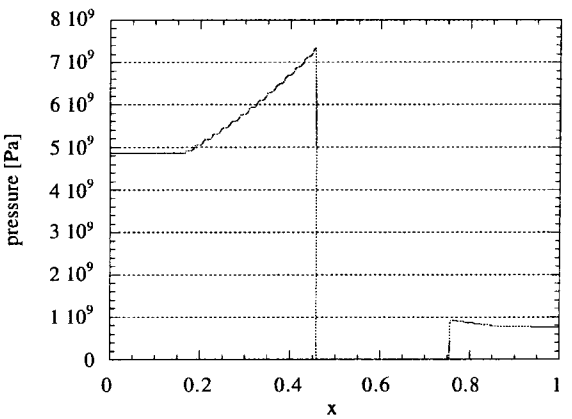


(b)

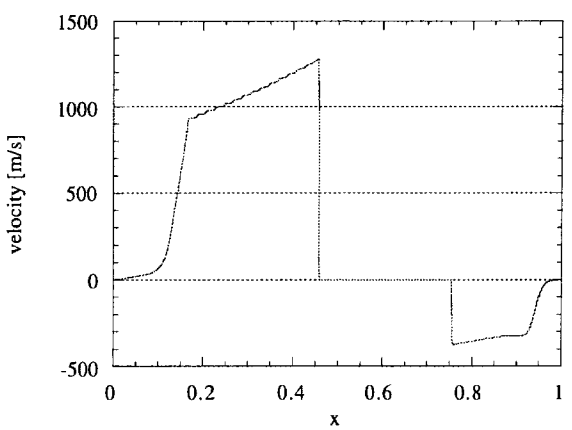


(c)

Figure 7. Flow field at $t = 57.8$ (μs).

 

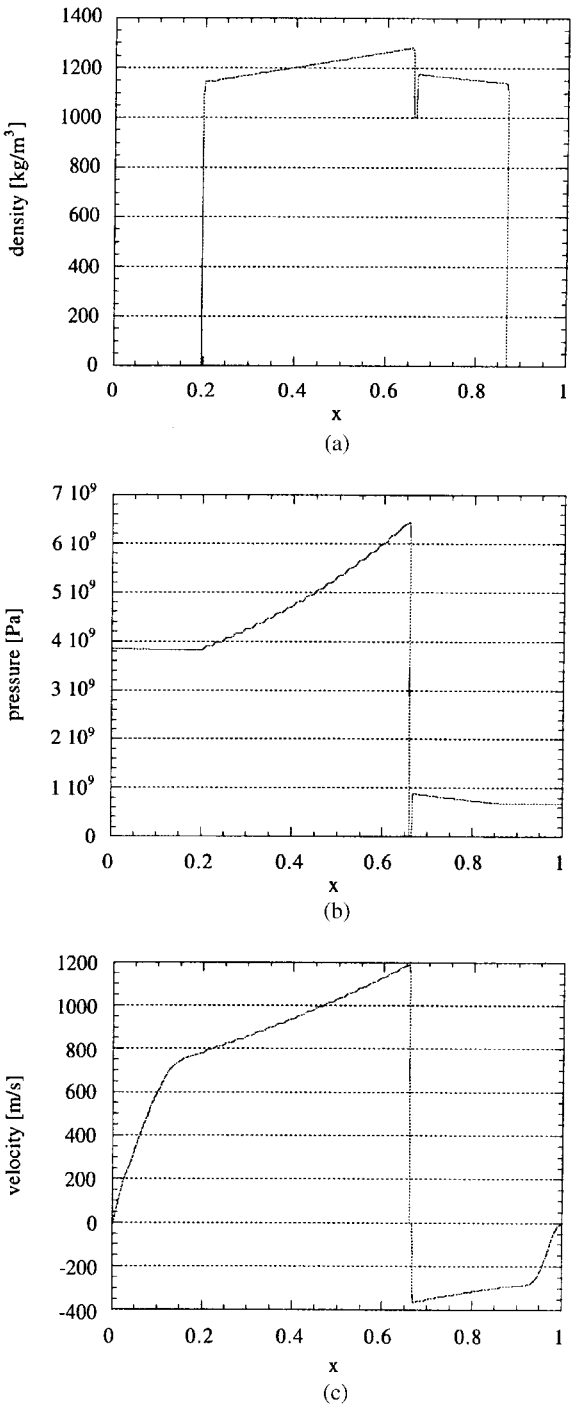


Figure 8. Flow field at $t = 94$ (μs).

 

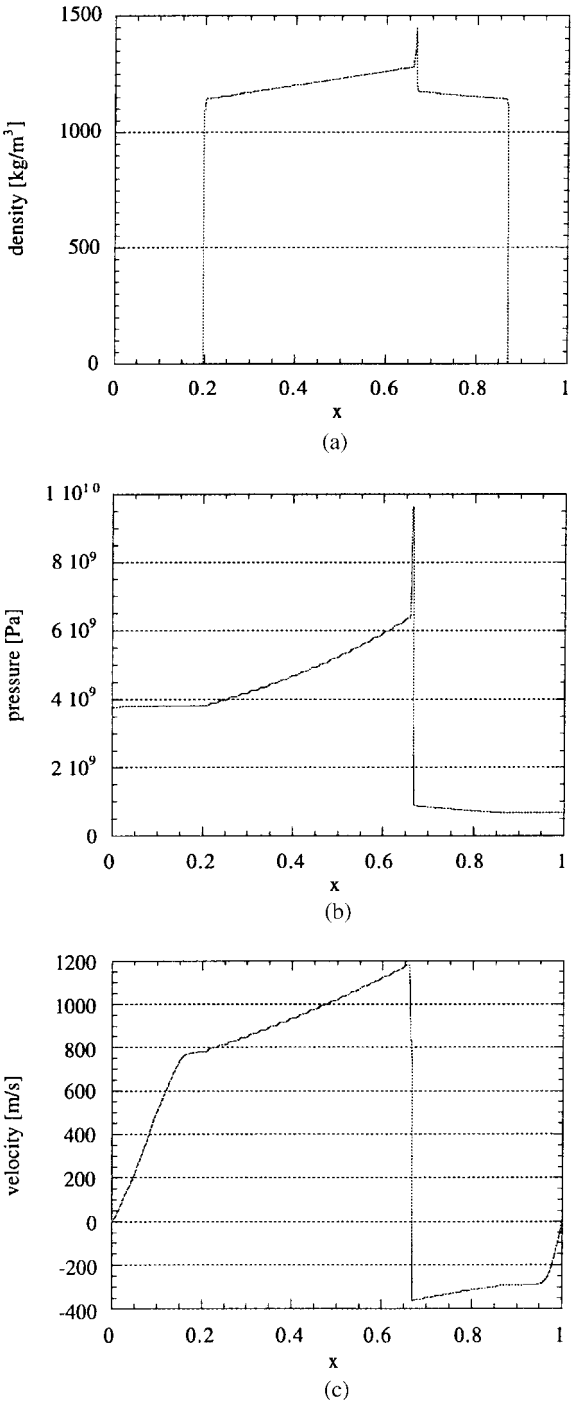


Figure 9. Flow field at $t = 95.5$ (μs).

 

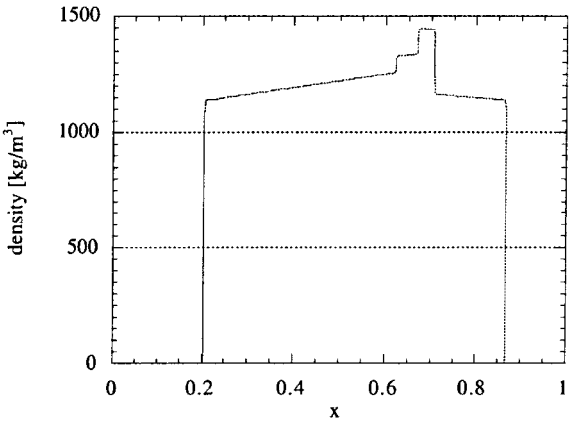


(a)

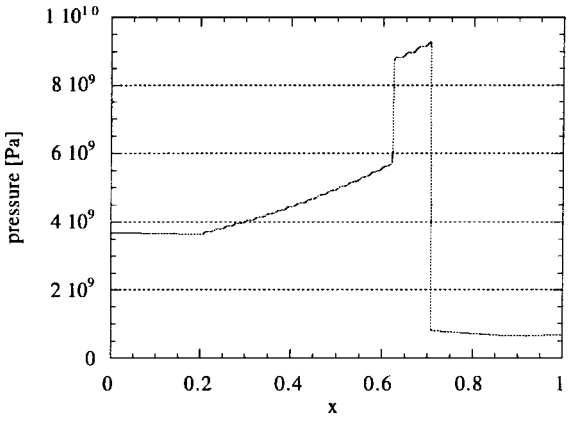


(b)

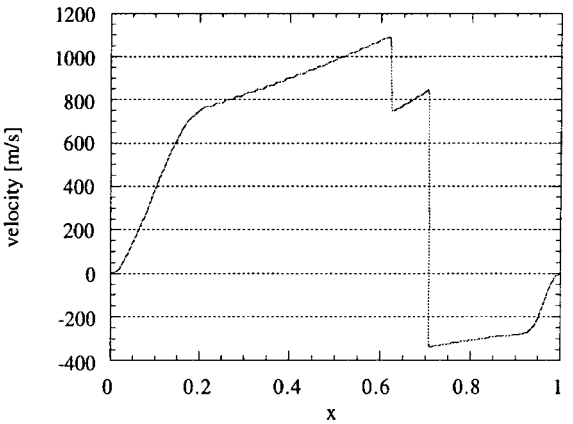


(c)

Figure 10. Flow field at $t = 102.5$ (μs).

 

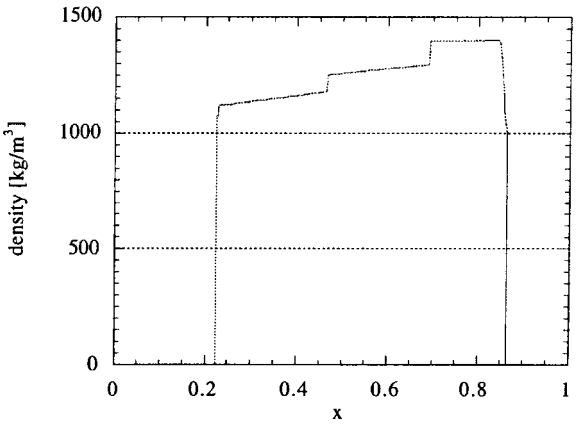


(a)

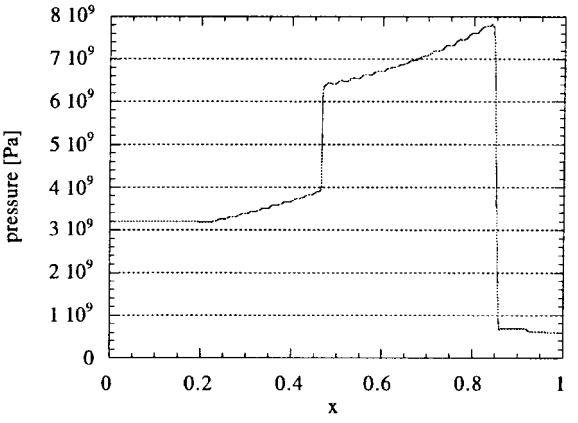


(b)

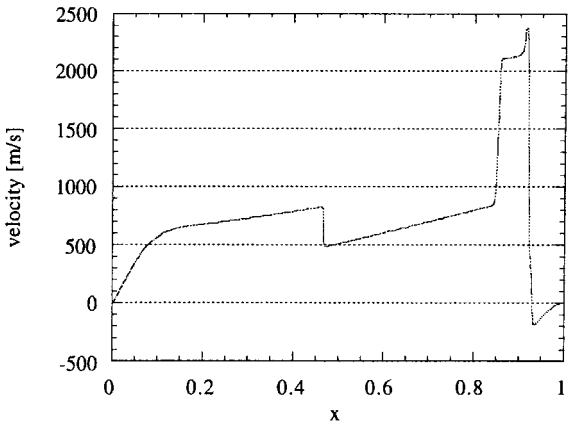


(c)

Figure 11. Flow field at $t = 131.2$ (μs).

 

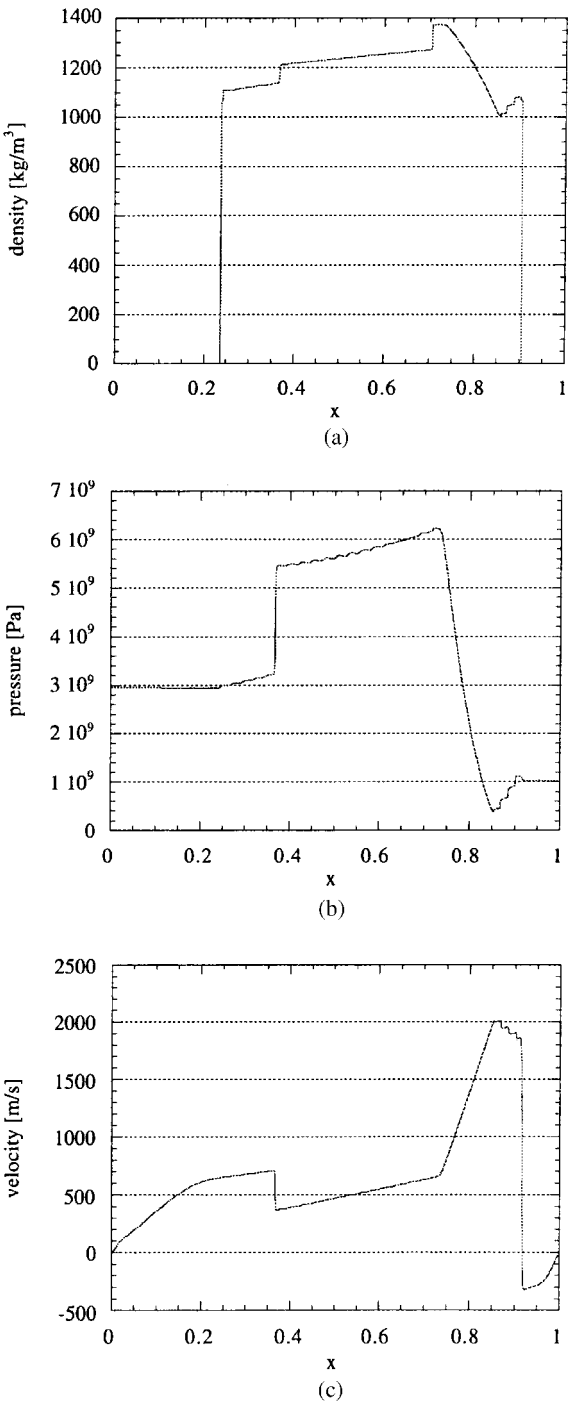


Figure 12. Flow field at $t = 151.5$ (μs).

 

Solutions of test examples have been presented and this scheme converged to the exact solution. Also presented is an example of two blast waves generated in air and interacting in water. This interaction resulted in a complex wave patterns which was handled nicely by the proposed scheme.

This scheme will be extended to two dimensional flow fields containing gas liquid interfaces.

ACKNOWLEDGEMENTS

The first author would like to acknowledge the Tohoku Kaihatsu Memorial Foundation for their financial support. Thanks are also due to Prof. E. F. Toro for his useful comments and suggestions and to Mr. Kosugi who helped the author to generate the figures given in the third example.

REFERENCES

1. Abgrall R. How to prevent pressure oscillations in multicomponent flow calculations: a quasi conservative approach. *Journal of Computational Physics* 1996; **125**:150–160.
2. Cocchi J, Saurel R. A Riemann problem based method for the resolution of compressible multimaterial flows. *Journal of Computational Physics* 1997; **137**:265–298.
3. Cocchi JP, Saurel R, Loraud JC. Treatment of interface problems with Godunov-type schemes. *Shock Waves* 1996; **5**:347–357.
4. Jenny P, Muller B, Thomann H. Correction of conservative Euler solvers for gas mixtures. *Journal of Computational Physics* 1997; **132**:91–107.
5. Karni S. Multicomponent flow calculations by a consistent primitive algorithm. *Journal of Computational Physics* 1994; **112**:31–43.
6. Karni S. Hybrid multifluid algorithms. *SIAM Journal on Scientific Computing* 1996; **17**:1019–1039.
7. Shyue K. An efficient shock—capturing algorithm for compressible multicomponent problems. *Journal of Computational Physics* 1998; **142**:208–242.
8. Mulder W, Osher S, Sethian JA. Computing interface motion in compressible gas dynamics. *Journal of Computational Physics* 1992; **100**:209–228.
9. Menikoff R, Plohr B. The Riemann problem for fluid flow of real materials. *Reviews of Modern Physics* 1989; **61**:75–130.
10. Harten A. High resolution schemes for hyperbolic conservation laws. *Journal of Computational Physics* 1983; **49**:357–393.
11. Yee HC. Upwind and symmetric shock capturing schemes. NASA 89464, 1987.
12. Woodward P, Colella P. The numerical simulation of two-dimensional fluid flow with strong shocks. *Journal of Computational Physics* 1984; **54**:115–173.
13. Ivings MJ, Causon DM, Toro EF. On hybrid high resolution upwind methods for multicomponent flows. *Zeitschrift fur Angewandte Mathematik und Mechanik* 1997; **77**:645–668.

 